

High-frequency force balance technique for tall buildings: a critical review and some new insights

Xinzhong Chen^{*1}, Dae-Kun Kwon² and Ahsan Kareem²

¹National Wind Institute, Texas Tech University, USA
²NatHaz Modeling Lab., University of Notre Dame, USA

(Received March 6, 2010, Revised September 30, 2012, Accepted October 1, 2012)

Abstract. The high frequency force balance (HFFB) technique provides convenient measurements of integrated forces on rigid building models in terms of base bending moments and torque and/or base shear forces. These base moments or forces are then used to approximately estimate the generalized forces of building fundamental modes with mode shape corrections. This paper presents an analysis framework for coupled dynamic response of tall buildings with HFFB technique. The empirical mode shape corrections for generalized forces with coupled mode shapes are validated using measurements of synchronous pressures on a square building surface from a wind tunnel. An alternative approach for estimating the mean and background response components directly using HFFB measurements without mode shape corrections is introduced with a discussion on higher mode contributions. The uncertainty in the mode shape corrections and its influence on predicted responses of buildings with both uncoupled and coupled modal shapes are examined. Furthermore, this paper presents a comparison of aerodynamic base moment spectra with available data sets for various tall building configurations. Finally, e-technology aspects in conjunction with HFFB technique such as web-based on-line analysis framework for buildings with uncoupled mode shapes used in NALD (NatHaz Aerodynamic Loads Database) is discussed, which facilitates the use of HFFB data for preliminary design stages of tall buildings subject to wind loads.

Keywords: wind loads; wind tunnel tests; buildings; building design; structural dynamics; dynamic analysis; random

1. Introduction

The high frequency force balance (HFFB) technique has been recognized as an effective tool for quantifying generalized wind forces on tall buildings with uncoupled mode shapes. The determination of the generalized wind forces through measured base bending moments or torque on a rigid building model requires empirical mode shape corrections (e.g., Kareem and Cermak 1979, Tschanz and Davenport 1983, Vickery *et al.* 1985, Reinhold and Kareem 1986, Boggs and Peterka 1989, Xu and Kwok 1993, Zhou *et al.* 2002, Holmes *et al.* 2003, Chen and Kareem 2004). The generalized forces are then utilized to estimate the building dynamic response with given structural characteristics. For buildings with one-dimensional (1D) mode shapes, building response

*Corresponding author, Professor, E-mail: xinzhong.chen@ttu.edu

in each primary direction can be evaluated separately without the consideration of cross-correlation of wind loads in different directions.

Buildings with complex geometric shapes or with structural systems having noncoincident centers of mass and rigidity, or both, generally exhibit three-dimensional (3D) coupled mode shapes and experience coupled responses when exposed to wind loads. Furthermore, the fundamental modal frequencies in three primary directions may be closely spaced. These situations warrant a 3D coupled response analysis framework which takes into account the cross correlation of wind loads in different directions and the intermodal coupling of modal responses. The correlation of two modal responses depends not only on the modal frequency ratio and damping ratios, but also on the coherence of the generalized wind forces, which differs from conventional uni-component earthquake excitations (Chen and Kareem 2005a, b). The HFFB measurements can be readily incorporated into the analysis frameworks when the mass centers of all floors lie on a single vertical axis and the mode shapes are assumed to be linear functions over the building height (Kareem 1985, Tallin and Ellingwood 1985, Shimada *et al.* 1990, Islam *et al.* 1992). The application of HFFB measurements to buildings with general 3D coupled modes have been studied in Irwin and Xie (1993), Yip and Flay (1995), Holmes *et al.* (2003), and Chen and Kareem (2005a, b). The modeling of equivalent static wind loads (ESWLs) for coupled building responses has been addressed in Chen and Kareem (2005a, b).

In this paper, the framework for the analysis of 3D coupled dynamic response of tall buildings with HFFB technique (Chen and Kareem 2005a, b) is revisited. The empirical mode shape corrections currently used in practice are validated using measurements of synchronous pressures on a square building surface from a wind tunnel. An alternative approach is also introduced for estimating the mean and background response components directly using the HFFB measurements without mode shape corrections. The uncertainty in the mode shape correction and its influence on building responses with both uncoupled and coupled mode shapes are examined. Furthermore, this paper presents a comparison of aerodynamic base moment spectra with available data sets for various tall building configurations. Finally, e-technology aspects in conjunction with HFFB technique such as web-based on-line analysis framework for buildings with uncoupled mode shapes used in NALD (NatHaz Aerodynamic Loads Database) is discussed, which facilitates the use of HFFB data for preliminary design stages of tall buildings subject to wind loads.

2. Analysis of coupled building response

A wind-excited tall building at a given wind speed and direction is considered for analysis. A Cartesian coordinate system with two orthogonal translational axes x and y and vertical axis z with the origin at the ground is used for describing the building system (Fig. 1). The i th floor of the building at the elevation z_i above the ground has a lumped mass m_i , and a polar moment of inertia I_i about the mass center of the floor ($i = 1, 2, \dots, N; N =$ total floor number). The centers of mass and rigidity of the i th floor are located at the points with the coordinates $(x, y, z) = (e_{ix}, e_{iy}, z_i)$, and $(x, y, z) = (e_{ixr}, e_{iyr}, z_i)$, respectively. The centers of geometry, mass and rigidity may not be coincident, and those at different floors may not be located on a single vertical line. The integrated wind loads in terms of the base bending moments along the axes x and y , and base torque about the axis z , i.e., $M_x(t)$, $M_y(t)$ and $M_\theta(t)$, are determined using the HFFB technique in a wind tunnel. The HFFB is attached to the base of the building model at the coordinate origin.

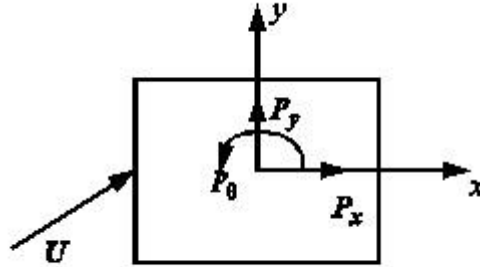


Fig. 1 Coordinate system and wind orientation

The building response can be estimated using modal analysis involving only the three fundamental modes. The j th ($j = 1,2,3$) mode shape in terms of the building motions at the i th floor point $(x, y, z) = (0,0, z_i)$ in three primary directions are denoted as Θ_{ijx} , Θ_{ijy} , and $\Theta_{ij\theta}$. The j th generalized force is expressed in terms of unknown 3D dynamic loading as

$$Q_j(t) = \sum_{i=1}^N \left(\Theta_{ijx} P_{ix}(t) + \Theta_{ijy} P_{iy}(t) + \Theta_{ij\theta} P_{i\theta}(t) \right) \quad (1)$$

where $P_{ix}(t)$, $P_{iy}(t)$, and $P_{i\theta}(t)$ = wind loading of the i th floor at the point $(x, y, z) = (0, 0, z_i)$ in three directions.

The mean and root-mean-square (RMS) value of the j th generalized displacement, \bar{q}_j and σ_{q_j} are calculated as

$$\bar{q}_j = \frac{\bar{Q}_j}{K_j} \quad (2)$$

$$\sigma_{q_j}^2 = \int_0^\infty |H_j(f)|^2 S_{Q_{jj}}(f) df \quad (3)$$

$$H_j(f) = \frac{1}{M_j(2\pi f_j)^2 \left[1 - (f/f_j)^2 + (2i\xi_j f)/f_j \right]} \quad (4)$$

$$M_j = \sum_{k=1}^N (m_k \Theta_{kjxc}^2 + m_k \Theta_{kjsc}^2 + I_k \Theta_{kj\theta c}^2) \quad (5)$$

where M_j , $K_j = M_j(2\pi f_j)^2$, f_j and ξ_j = j th generalized mass, stiffness, frequency and damping ratio; $\Theta_{kjxc} = \Theta_{kix} - e_{ky} \Theta_{kj\theta}$, $\Theta_{kjsc} = \Theta_{kijy} + e_{kx} \Theta_{kj\theta}$, $\Theta_{kjxc} = \Theta_{kj\theta}$ = motions at the mass center of the k th floor in j th mode; \bar{Q}_j and $S_{Q_{jj}}(f)$ = the mean and power spectrum density (PSD) function of $Q_j(t)$; f = frequency; and $i = \sqrt{-1}$.

The correlation coefficient between the j th and k th modal responses, r_{jk} , is given by

$$r_{jk} = \frac{\text{Re} \left[\int_0^\infty H_j(f) H_k^*(f) S_{Q_{jk}}(f) df \right]}{\sigma_{q_j} \sigma_{q_k}} \tag{6}$$

where $S_{Q_{jk}}(f)$ = cross power spectral density (XPSD) function between $Q_j(t)$ and $Q_k(t)$; Re and * = real and complex conjugate operators, respectively.

It is often convenient to separate the modal response into background and resonant components, which can be estimated using the following closed-form formulations (e.g., Chen and Kareem 2005a, b)

$$\sigma_{q_j}^2 = \sigma_{q_{jb}}^2 + \sigma_{q_{jr}}^2 \tag{7}$$

$$\sigma_{q_{jb}}^2 = \int_0^{f'} |H_j(f)|^2 S_{Q_{jj}}(f) df \approx \frac{1}{K_j^2} \int_0^\infty S_{Q_{jj}}(f) df = \frac{\sigma_{Q_j}^2}{K_j^2} \tag{8}$$

$$\sigma_{q_{jr}}^2 = \int_{f'}^\infty |H_j(f)|^2 S_{Q_{jj}}(f) df \approx \frac{1}{K_j^2} \frac{\pi}{4\xi_j} f_j S_{Q_{jj}}(f_j) \tag{9}$$

$$r_{jk} = (r_{jkb} \sigma_{q_{jb}} \sigma_{q_{kb}} + r_{jkr} \sigma_{q_{jr}} \sigma_{q_{kr}}) / (\sigma_{q_j} \sigma_{q_k}) \tag{10}$$

$$r_{jkb} \approx r_{Q_{jk}} = \int_0^\infty \text{Re}[S_{Q_{jk}}(f)] df / (\sigma_{q_j} \sigma_{q_k}) \tag{11}$$

$$r_{jkr} = \alpha_{jkr} \rho_{jkr} \tag{12}$$

$$\alpha_{jkr} = \text{Re}[S_{Q_{jk}}(f)] / \sqrt{S_{Q_{jj}}(f) S_{Q_{kk}}(f)} \Big|_{f=\frac{f_j+f_k}{2}} \tag{13}$$

$$\rho_{jkr} = \frac{8\sqrt{\xi_j \xi_k} (\beta_{jk} \xi_j + \xi_k) \beta_{jk}^{3/2}}{(1 - \beta_{jk}^2)^2 + 4\xi_j \xi_k \beta_{jk} (1 + \beta_{jk}^2) + 4(\xi_j^2 + \xi_k^2) \beta_{jk}^2} \tag{14}$$

where f' = a frequency less than the lowest fundamental modal frequency; σ_{q_j} = RMS value of $Q_j(t)$; $r_{Q_{jk}}$ = correlation coefficient between $Q_j(t)$ and $Q_k(t)$; $\beta_{jk} = f_j/f_k$ = modal frequency ratio; ξ_j and ξ_k = modal damping ratios; and the subscripts b and r denote background and resonant components, respectively.

Once the generalized displacement is quantified, any response of interest, e.g., displacement, bending moment, shear force, and other member forces at any building elevations can be accordingly determined. The mean and RMS value (including the background and resonant components) of a specific response $R(t)$ are estimated as

$$\bar{R} = \sum_{j=1}^3 \bar{R}_j = \sum_{j=1}^3 \Gamma_j \bar{q}_j \tag{15}$$

$$\sigma_R^2 = \sum_{j=1}^3 \sum_{k=1}^3 \sigma_{R_j} \sigma_{R_k} r_{jk} = \sum_{j=1}^3 \sum_{k=1}^3 \Gamma_j \Gamma_k \sigma_{q_j} \sigma_{q_k} r_{jk} \tag{16}$$

where Γ_j = j th modal participation coefficient for R , representing the response of R under the modal inertial load with a unit generalized displacement, i.e.,

$$\Gamma_j = \sum_{i=1}^N (\mu_{ix} F_{ijx0} + \mu_{iy} F_{ijy0} + \mu_{i\theta} F_{ij\theta 0}) \tag{17}$$

$$F_{ijx0} = (2\pi f_j)^2 m_i \Theta_{ijxc} \tag{18}$$

$$F_{ijy0} = (2\pi f_j)^2 m_i \Theta_{ijyc} \tag{19}$$

$$F_{ij\theta 0} = (2\pi f_j)^2 (-m_i e_{iy} \Theta_{ijxc} + m_i e_{ix} \Theta_{ijyc} + I_i \Theta_{ij\theta c}) \tag{20}$$

F_{ijx0} , F_{ijy0} and $F_{ij\theta 0}$ = j th 3D modal inertial load with a unit generalized displacement at the i th floor point $(x, y, z) = (0, 0, z_i)$; μ_{ix} , μ_{iy} , and $\mu_{i\theta}$ = 3D influence coefficients of $R(t)$, representing the response of R under a unit load at the i th floor in three directions, respectively.

It is evident that for the displacement at the i th floor point $(x, y, z) = (0, 0, z_i)$ in the axis s ($s = x, y, \theta$) direction, Γ_j is given by Θ_{ijs} . For shear forces, bending moments and torque (about axis z) at the i th floor, Γ_j are respectively expressed as

$$\Gamma_j = \sum_{k=i+1}^N (2\pi f_j)^2 m_k \Theta_{kjsc} \quad (s = x, y) \tag{21}$$

$$\Gamma_j = \sum_{k=i+1}^N (z_k - z_i) (2\pi f_j)^2 m_k \Theta_{kjsc} \quad (s = x, y) \tag{22}$$

$$\Gamma_j = \sum_{k=i+1}^N (2\pi f_j)^2 (-m_k e_{ky} \Theta_{kjsc} + m_k e_{kx} \Theta_{kjyc} + I_k \Theta_{kj\theta c}) \tag{23}$$

The acceleration response is calculated by considering only the resonant component. For the acceleration at the i th floor point $(x, y, z) = (0, 0, z_i)$ along axis s ($s = x, y, \theta$), Γ_j is given by $(2\pi f_j)^2 \Theta_{ijs}$.

The correlation coefficient between two response components, $R(t)$ and $D(t)$, is given by

$$r_{RD} = \sum_{j=1}^3 \sum_{k=1}^3 \Gamma_j \Gamma_{kD} \sigma_{q_j} \sigma_{q_k} r_{jk} / (\sigma_R \sigma_D) \tag{24}$$

where σ_D = RMS value of response $D(t)$ and given by Eq. (16) with Γ_k replaced by Γ_{kD} ; and Γ_{kD} = k th modal participation coefficient for $D(t)$.

The peak value of $R(t)$ during a time duration is then estimated as $\bar{R} \pm g \sigma_R$, where g is the peak factor given as

$$g = \sqrt{2 \ln(v_0 T)} + \frac{0.5772}{\sqrt{2 \ln(v_0 T)}} \tag{25}$$

where $v_0 = \sigma_{\dot{R}} / (2\pi \sigma_R)$ = upcrossing rate at zero mean; $\sigma_{\dot{R}}$ = RMS value of derivative of $R(t)$; and T = time duration.

In building design, the peak value of a resultant response $E(t)$ contributed from two responses $R(t)$ and $D(t)$ is of concern. One example is the absolute acceleration at a given location regardless of direction as a sum of squares of two translational components. The peak value of the resultant response

$$E = \sqrt{R^2 + D^2} \quad (26)$$

can be estimated as follows (Chen and Huang 2009)

$$E_{\max} = \max\{E_{\max 1}, E_{\max 2}\}$$

$$E_{\max 1} = \sqrt{\frac{|R|_{\max}^2 + |D|_{\max}^2}{2} + \sqrt{\left(\frac{|R|_{\max}^2 - |D|_{\max}^2}{2}\right)^2 + r_{RD}^2 |R|_{\max}^2 |D|_{\max}^2}} \quad (27)$$

$$E_{\max 2} = 0.8\sqrt{|R|_{\max}^2 + |D|_{\max}^2}$$

where $|R|_{\max}$ and $|D|_{\max}$ = peak values of dynamic components of $|R(t)|$ and $|D(t)|$, which can be estimated using the peak factor approach with the upcrossing rate ν_0 replaced by $2\nu_0$.

3. Mode shape corrections for generalized forces

The generalized wind forces used in the aforementioned framework are estimated from the HFFB measurements. To address the mode shape corrections, the measured base bending moments and torque are expressed by the unknown 3D wind forces at different floor levels as

$$M_x(t) = \sum_{i=1}^N z_i P_{ix}(t); \quad M_y(t) = \sum_{i=1}^N z_i P_{iy}(t); \quad M_\theta(t) = \sum_{i=1}^N P_{i\theta}(t) \quad (28)$$

On the other hand, the j th generalized force $Q_j(t)$ given by Eq. (1) is represented in its components as

$$Q_j(t) = Q_{jx}(t) + Q_{jy}(t) + Q_{j\theta}(t) \quad (29)$$

$$Q_{jx}(t) = \sum_{i=1}^N \theta_{ijx} P_{ix}(t); \quad Q_{jy}(t) = \sum_{i=1}^N \theta_{ijy} P_{iy}(t); \quad Q_{j\theta}(t) = \sum_{i=1}^N \theta_{ij\theta} P_{i\theta}(t) \quad (30)$$

The PSD of $Q_j(t)$, $S_{Q_{jj}}(f)$, and the XPSD between $Q_j(t)$ and $Q_k(t)$, $S_{Q_{jk}}(f)$, are expressed in terms of the spectra of their components as

$$S_{Q_{jj}}(f) = \sum_{s=x,y,\theta} \sum_{l=x,y,\theta} S_{Q_{jjsl}}(f) \quad (31)$$

$$S_{Q_{jk}}(f) = \sum_{s=x,y,\theta} \sum_{l=x,y,\theta} S_{Q_{jksl}}(f) \quad (32)$$

where $S_{Q_{jjsl}}(f)$ and $S_{Q_{jksl}}(f) =$ XPSDs between $Q_{js}(t)$ and $Q_{jl}(t)$, and between $Q_{js}(t)$ and $Q_{kl}(t)$.

For a general 3D mode shape with nonlinear variations in the translational directions and nonuniform variation in torsion, the PSD of $Q_{js}(t)$, i.e., $S_{Q_{js}}(f) = S_{Q_{jjss}}(f)$, can be estimated from the PSD of the corresponding base bending moment or torque $M_s(t)$ ($s = x, y, \theta$), i.e., $S_{M_s}(f) = S_{M_{ss}}(f)$, as

$$S_{Q_{js}}(f) = \eta_{js}^2(f) S_{M_s}(f) \quad (s = x, y, \theta) \quad (33)$$

where $\eta_{js}(f)$ ($j = 1, 2, 3; s = x, y, \theta$) = mode shape corrections for estimating the generalized force component $Q_{js}(t)$ from $M_s(t)$.

The wind loads at different building elevations but in the same direction are often assumed to be in-phase or out-of-phase. This results in real-valued mode shape corrections. Consequently, the XPSDs of the generalized force components, i.e., $S_{Q_{jjsl}}(f)$ and $S_{Q_{jksl}}(f)$ in Eqs. (31) and (32), can be estimated from the XPSDs of the corresponding measured base moments and torque as

$$S_{Q_{jjsl}}(f) = \eta_{js}(f) \eta_{jl}(f) S_{M_{sl}}(f) \quad (34)$$

$$S_{Q_{jksl}}(f) = \eta_{js}(f) \eta_{kl}(f) S_{M_{sl}}(f) \quad (35)$$

where $S_{M_{sl}}(f) =$ XPSD between measured $M_s(t)$ and $M_l(t)$ ($s, l = x, y, \theta$).

From the definitions of the total of nine mode shape corrections, it is evident that these mode shape corrections can be estimated using the same formulations adopted in the 1D uncoupled case. In the case of 3D coupled modes, the cross correlations or XPSDs of base bending moments and torque also play an important role in the calculation of the generalized forces. The quantification of mode shape corrections has to rely on empirical correction or analytical formulations derived based on a presumed analytical wind loading model. For example, when the XPSD of wind loads acting in the s direction at i th and k th floors, i.e., $S_{P_{ikss}}(f)$, and the component of the j th mode shape in the s direction are described by

$$S_{P_{ikss}}(f) = \frac{S_{P_{s0}}(f)}{H^2} \left(\frac{z_i}{H}\right)^{\alpha_s} \left(\frac{z_k}{H}\right)^{\alpha_s} \exp\left(-\frac{k_{zs} f |z_i - z_k|}{U_H}\right) \quad (36)$$

$$\Theta_{ijs} = \Theta_{js0} \left(\frac{z_i}{H}\right)^{\beta_{js}} \quad (37)$$

the mode shape correction defined as

$$\eta_{js}^2(f) = \frac{\sum_{i=1}^N \sum_{k=1}^N \Theta_{ijs} \Theta_{kjs} S_{P_{ikss}}(f)}{\sum_{i=1}^N \sum_{k=1}^N z_i^{\beta_s'} z_k^{\beta_s'} S_{P_{ikss}}(f)} \quad (38)$$

can be estimated using the following closed-form expression (Chen and Kareem 2004)

$$\eta_{js} = \frac{\Theta_{js0} (1 + \alpha_s + \beta'_s)}{H\beta'_s (1 + \alpha_s + \beta_{js})} \sqrt{\frac{1 + k_{zs}fH/U_H/(2.5 + \beta'_s)}{1 + k_{zs}fH/U_H/(2.5 + \beta_{js})}} \quad (39)$$

where $S_{P_{s0}}(f)$ = PSD of wind load at the building top; k_{zs} = decay factor; U_H = mean wind speed at the building top; H = building height; α_s = exponent of wind load profile; β_{js} = j th mode shape exponent of the s component; $\beta'_s = 1$ for $s = x, y$; and $\beta'_s = 0$ for $s = \theta$. When $k_{zs}fH/U_H \rightarrow 0$, which corresponds to full coherence of wind loads, the mode shape correction is the same as suggested in Xu and Kwok (1993) and discussed in Holmes *et al.* (2003). It should be noted that when the actual building mode shape departs distinctly from a power law variation, the mode shape correction calculated based on its definition given by Eq. (38) using the actual mode shape will lead to a better estimation rather than the closed-form formulation.

The following mode shape corrections were suggested by Holmes *et al.* (2003)

$$\eta_{js} = \frac{\Theta_{js0}}{H} \sqrt{\frac{4}{1 + 3\beta_{js}}} \quad (s = x, y) \quad (40)$$

$$\eta_{j\theta} = \Theta_{j\theta 0} \sqrt{\frac{1}{1 + 2\beta_{j\theta}}} \quad (41)$$

In Xie and Irwin (1998), instead of using the empirical mode shape corrections, the HFFB measurements were directly used to quantify an empirical loading model. For example, the wind pressure at elevation z above the ground along x direction, i.e., $p_x(z, t)$, was assumed to follow a linear variation over the building height as

$$p_x(z, t) = p_{0x}(t) + p_{1x}(t) \left(\frac{z}{H}\right) \quad (42)$$

where $p_{0x}(t)$ and $p_{1x}(t)$ are determined from the measured base shear force and bending moment, i.e., $F_x(t)$ and $M_x(t)$. Accordingly, the generalized wind force component, i.e., $Q_{jx}(t)$, associated with the mode shape $\Theta_{jx}(z) = \Theta_{jx0}(z/H)^{\beta_{jx}}$ of a building with a uniform width, B , is then calculated from $F_x(t)$ and $M_x(t)$ in the time domain as

$$Q_{jx}(t) = \frac{\Theta_{jx0}}{H(1 + \beta_{jx})(2 + \beta_{jx})} [2(1 - \beta_{jx})F_x(t)H + 6\beta_{jx}M_x(t)] \quad (43)$$

and in the frequency domain as

$$S_{Q_{jx}}(f) = \frac{\Theta_{jx0}^2}{H^2(1 + \beta_{jx})^2(2 + \beta_{jx})^2} \left(4(1 - \beta_{jx})^2 H^2 S_{F_x}(f) + 24(1 - \beta_{jx})\beta_{jx} H \text{Re}[S_{F_x M_x}(f)] + 36\beta_{jx}^2 S_{M_x}(f) \right) \quad (44)$$

where $S_{F_x}(f)$ and $S_{M_x}(f)$ = PSDs of $F_x(t)$ and $M_x(t)$; and $S_{F_x M_x}(f)$ = XPSD between $F_x(t)$ and $M_x(t)$.

4. An alternative approach for mean and background responses

In the aforementioned approach, the mean and background response components are determined from the generalized forces using the same modal shape corrections as the resonant component. In the following, an alternative approach is presented for estimating the mean and background response components without the mode shape corrections. The HFFB technique provides direct measurements of the mean and background components of the base bending moments and torque. These can be used to estimate the mean and background components of the generalized displacements and other responses. Assuming the mean and background responses are contributed from only the three fundamental modes, the mean and RMS values of the base bending moments and torque are expressed in terms of the generalized displacements as

$$\bar{M}_s = \sum_{j=1}^3 \Gamma_{jM_s} \bar{q}_j \quad (s = x, y, \theta) \quad (45)$$

$$\sigma_{M_s}^2 = \sum_{j=1}^3 \sum_{k=1}^3 \Gamma_{jM_s} \Gamma_{kM_s} r_{jkb} \sigma_{q_{jb}} \sigma_{q_{kb}} \quad (s = x, y, \theta) \quad (46)$$

$$r_{sl} \sigma_{M_s} \sigma_{M_l} = \sum_{j=1}^3 \sum_{k=1}^3 \Gamma_{jM_s} \Gamma_{kM_l} r_{jkb} \sigma_{q_{jb}} \sigma_{q_{kb}} \quad (s, l = x, y, \theta) \quad (47)$$

where Γ_{jM_s} ($j = 1, 2, 3; s = x, y, \theta$) = j th modal participation coefficient for $M_s(t)$; and r_{sl} ($s, l = x, y, \theta$) = correlation coefficient between $M_s(t)$ and $M_l(t)$.

Accordingly, the mean and background displacements are determined as

$$\{\bar{q}\} = [\Gamma]^{-1} \{\bar{M}\}; \quad [\Pi_{q_b}] = [\Gamma]^{-1} [\Pi_M] [\Gamma]^{-T} \quad (48)$$

where $\{\bar{q}\} = \{\bar{q}_1, \bar{q}_2, \bar{q}_3\}^T$; $\{\bar{M}\} = \{\bar{M}_x, \bar{M}_y, \bar{M}_\theta\}^T$; $[\Gamma] = [\Gamma_{jM_s}] = 3$ by 3 modal participation coefficient matrix of the base bending moments and torque; $[\Pi_M] = [r_{sl} \sigma_{M_s} \sigma_{M_l}]$ and $[\Pi_{q_b}] = [r_{jkb} \sigma_{q_{jb}} \sigma_{q_{kb}}] = 3$ by 3 covariance matrices of the base bending moments and torque, and the generalized background displacements.

5. Validation of mode shape corrections

To evaluate the accuracy of the mode shape corrections currently used in practice, a tall square building with 40 m square in plane and 200 m in height is considered. The spatio-temporarily varying pressures on the building surface were obtained using a 1/400 scaled building model in a wind tunnel with a multiple channel pressure scanning system (MPS) (Tamura *et al.* 1999). A total of 500 wind pressure taps with 25 rows were uniformly distributed over four wall surfaces of the model. The wind tunnel experiment was carried out for a suburban terrain with a power law exponent of mean wind speed profile of 1/6. The wind direction was set normal to the wall face,

i.e., along axis x . The Cartesian coordinate system is defined with the vertical axis z through the geometric center of the building section. Fig. 2 shows the mean and RMS local wind force coefficients over the building height. The mean wind force coefficient in alongwind direction increases with the building height, while those in crosswind and torsional directions are close to zero. The RMS wind force coefficients in alongwind and torsional directions are almost constant over the building height. The RMS wind force coefficient in crosswind direction increases with building elevation until about 65% of the building height and then decreases.

The base bending moments and torque are calculated from the building surface pressures and are regarded as the HFFB measurements. The alongwind and acrosswind base shear forces are also calculated. Fig. 3 shows the PSDs of the alongwind and acrosswind base bending moments and base torque. The peaks in the PSDs of the crosswind base bending moment and base torque are associated with vortex shedding. The correlations of alongwind loads with crosswind and torsional loads are negligible, while the correlation between the crosswind and torsional loads is significant. The base bending moments, base torque and base shear forces are normalized by dividing $0.5\rho U_H^2 B H^2$, $0.5\rho U_H^2 B^2 H$, and $0.5\rho U_H^2 B H$, respectively, for defining the corresponding non-dimensional coefficients. The mean alongwind base bending moment and shear force coefficients are 0.589 and 1.094. The RMS coefficients for alongwind base bending moment and base shear, crosswind base bending moment and shear, and base torque are 0.111 and 0.208, 0.160 and 0.308, and 0.037, respectively.

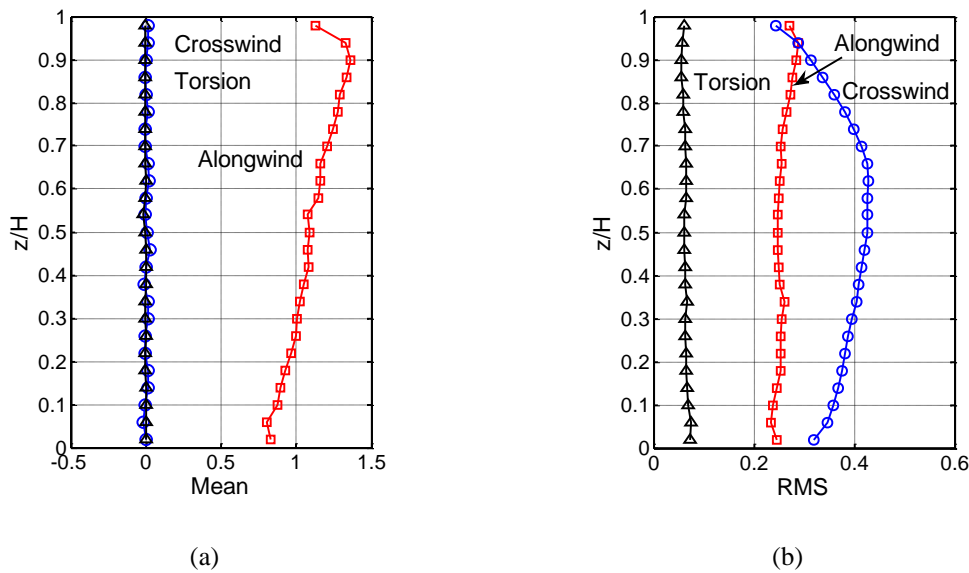


Fig. 2 Mean and RMS local wind force coefficients over the building height

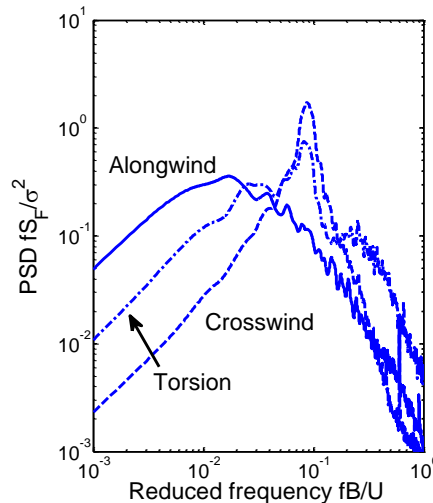
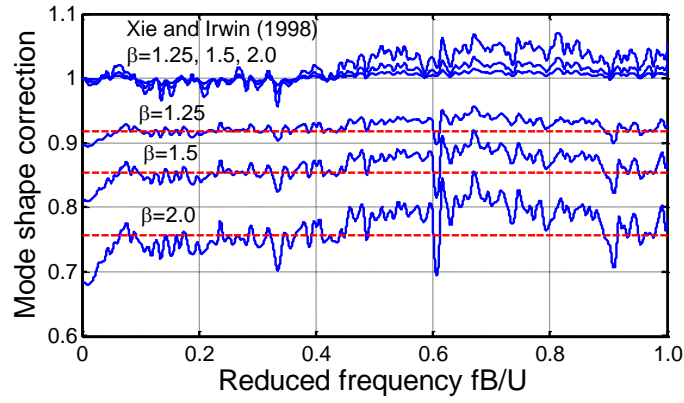


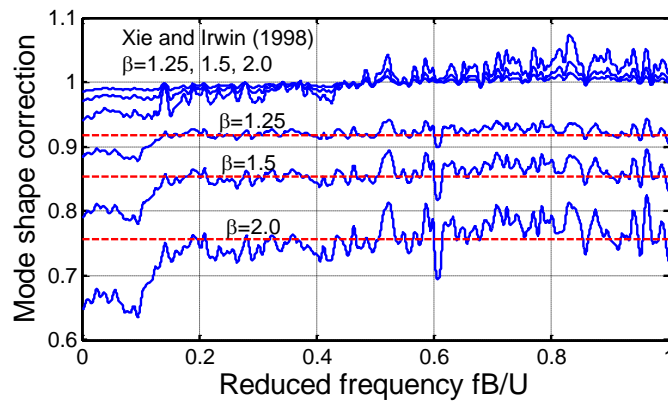
Fig. 3 PSDs of base bending moments and torque

From the PSDs of the base bending moments and torque and those of the generalized wind forces with power law mode shapes, the required mode shape corrections are calculated as shown in Fig. 4. The empirical values suggested by Holmes *et al.* (2003) are also compared. For the translational modes, the generalized forces estimated using the scheme by Xie and Irwin (1998), which does not involve mode shape correction, are also calculated. The ratios of the roots of their PSDs to those of the actual generalized forces are also shown in Fig. 4. It is seen that the empirical mode shape corrections for translational modes perform very well. The generalized forces determined from the scheme by Xie and Irwin (1998) are in good agreement with the actual ones, while it requires simultaneous measurements of both base shear and moment rather than the base bending moment only in traditional HFFB technique. The good performance of the mode shape corrections for translational modes are due, in part, to the similarity of the linear influence function of the base bending moment to the translational mode shape. On the other hand, in the case of torsional mode, as the uniform influence function of the base torque differs distinctly from the mode shape, a considerable correction with a relatively larger uncertainty is needed for the calculation of the generalized force from the base torque. For this specific case, it is shown that the correction factor of 0.7 is too conservative, while the value suggested in Holmes *et al.* (2003) leads to an under-estimation over the reduced frequency range from $fB/U_H = 0.3$ to 1.0.

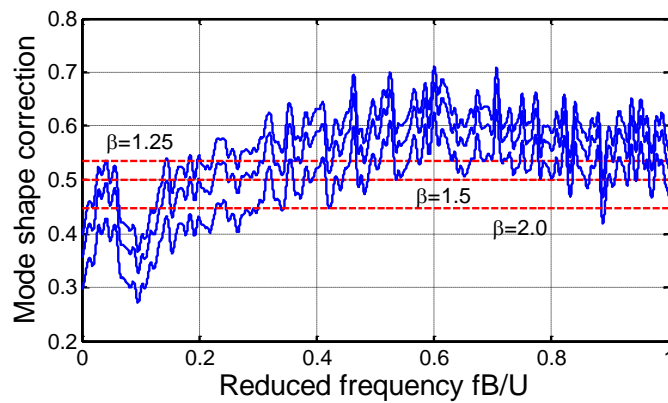
The phase spectra between the base bending moment or torque and the corresponding generalized forces are calculated for each primary direction. While it is not shown here, the almost zero phase over the entire reduced frequency range indicates that the base bending moment or torque are in-phase with the corresponding generalized force. That demonstrates that the mode shape corrections can be regarded as real-valued, and the cross correlations of the base bending moments and torque accurately represent the cross correlations of the generalized force components in different directions.



(a) Alongwind



(b) Crosswind



(c) Torsion

Fig. 4 Comparison of mode shape corrections

6. Influence of mode shape corrections on building responses: uncoupled case

The square tall building with the coincident centers of geometry, mass and rigidity is considered. The building mass intensity is 192 kg/m^3 . The radius of gyration is 12.656 m. The fundamental frequencies of the translational modes and torsional mode are 0.23 Hz, 0.23 Hz and 0.3 Hz, respectively. The modal damping ratios are 1%. The mode shapes in primary directions are 1D uncoupled and are assumed to be identical following a power law with an exponent of 1.25. Table 1 summaries the mean, RMS background, RMS resonant and RMS total response components in terms of building top displacements, base bending moments and torque coefficients, and base shear force coefficients. Table 2 shows the RMS accelerations at the building top center and corner A: $(x, y) = (0.5B, 0.5B)$. The resultant accelerations at these two locations are also calculated using the combination scheme suggested in Chen and Huang (2009). The corresponding peak value can be estimated by further multiplying a peak factor. As the mean and background response components are proportional to the square of mean wind speed, the mean and background displacements at 40 m/s can be readily given from those at 20 m/s by multiplying a factor of 4. The non-dimensional mean and background base moment, torque and force coefficients remain constants for different mean wind speeds. On the other hand, the resonant response component grows fast than the square of mean wind speed due to dynamic amplification effect.

The predicted response from the HFFB technique with the mode shape corrections suggested in Holmes *et al.* (2003) are compared with those determined using the actual generalized forces, referred to as MPS approach. As expected, the alongwind and acrosswind responses from the HFFB technique are in good agreement with the MPS approach. On the other hand, the HFFB technique overestimates the background torsional displacement and base torque, but underestimates the resonant component at $U_H=20 \text{ m/s}$, i.e., reduced frequency $fB/U_H=0.6$ for the torsional mode. The torsional acceleration is underestimated by 22%. As a result, the acceleration at the corner A in x direction and the resultant acceleration are underestimated by 15% and 13%, respectively. On the other hand, at $U_H=40 \text{ m/s}$, i.e., $fB/U_H=0.3$, the torsional response from the HFFB technique is in a good agreement with those from the MPS approach.

The mean and background response components are also determined by directly using the base bending moments and base torque measurements without mode shape corrections, referred to as a direct approach. As the base bending moments and building top displacements are predominated by the contribution of the fundamental mode with negligible contributions from higher modes, these response quantities estimated from the MPS approach are in good agreement with those from the direct approach. The significance of higher mode contributions depends on the influence function of the response (Huang and Chen 2007). The top displacement and base bending moment are less sensitive to higher mode contributions. In particular, for buildings with a linear mode shape, the higher modes will provide no contribution to the base bending moment due to the orthogonality between the higher mode shapes and the influence function, although they would affect other response components. It is noted that when the spatiotemporally varying wind loading is available, the determination of mean and background responses using static and quasi-static analyses expressed in terms of influence functions are equivalent to involving all modal contributions. The higher mode contributions to the mean and background responses are more noticeable as compared to the resonant component.

Table 1 Comparison of the building responses (Uncoupled building, RMS)

Component	Approach	$X(cm)$	$Y(cm)$	$0.5B\theta(cm)$	CM_x	CM_y	CM_θ	CF_x	CF_y
$U_H = 20 m/s$									
Mean	MPS	2.833	0	0	0.583	0	0	0.841	0
	HFFB	2.772	0	0	0.570	0	0	0.823	0
	Direct	2.807	0	0	0.589	0	0	0.851	0
B	MPS	0.524	0.742	0.160	0.108	0.153	0.027	0.156	0.221
	HFFB	0.534	0.765	0.182	0.110	0.157	0.031	0.159	0.227
	Direct	0.540	0.775	0.218	0.111	0.159	0.037	0.161	0.230
R	MPS	0.392	0.508	0.265	0.081	0.104	0.045	0.117	0.151
	HFFB	0.359	0.470	0.204	0.074	0.097	0.034	0.107	0.140
Total	MPS	0.655	0.900	0.310	0.135	0.185	0.052	0.194	0.267
	HFFB	0.644	0.898	0.273	0.132	0.185	0.046	0.191	0.267
$U_H = 40 m/s$									
R	MPS	2.700	5.865	1.996	0.139	0.301	0.084	0.200	0.435
	HFFB	2.561	5.608	1.957	0.132	0.288	0.082	0.190	0.416
Total	MPS	3.415	6.574	2.100	0.176	0.338	0.088	0.254	0.488
	HFFB	3.335	6.389	2.088	0.171	0.328	0.088	0.248	0.474

Table 2 Comparison of the building accelerations (Uncoupled building, RMS, milli-g)

Approach	$(x,y) = (0,0)$				$(x,y) = (0.5B,0.5B)$				$0.5Ba_\theta$
	a_x	a_y	r_{xy}	$\sqrt{a_x^2 + a_y^2}$	a_x	a_y	r_{xy}	$\sqrt{a_x^2 + a_y^2}$	
$U_H = 20 m/s$									
MPS	0.827	0.973	-0.06	1.022	1.253	1.354	-0.55	1.626	0.946
HFFB	0.766	1.001	-0.09	1.008	1.064	1.246	-0.47	1.414	0.738
$U_H = 40 m/s$									
MPS	5.652	11.913	-0.05	11.913	9.200	14.031	-0.44	14.853	7.243
HFFB	5.468	11.951	-0.07	11.959	8.955	13.918	-0.44	14.693	7.097

For this building example, the RMS background shear force coefficients calculated by integrating the building surface pressures are 0.208 and 0.308, respectively, for alongwind and acrosswind directions. The largest values using the modal analysis are given by the direct method, which are 0.161 and 0.230 with underestimations of 23% and 25%, respectively. By the way, the mean base shear force coefficient predicted by modal analysis with the direct method is 0.851, which underestimates the actual value of 1.094 by 22%. Similar to the base shear force, the background base torque is also noticeably contributed by higher modes. The direct method treats the measured base torque, which actually includes all modal contributions, as the response of only the fundamental mode, thus leads to overestimates of the fundamental modal response and the background torsional top displacement. It should be mentioned that a use of 5-component load cell or equivalent in HFFB tests provides direct measurements of base shears along with base bending moments and base torque. The mean and background components of base shears derived from this method is considered more precise than the aforementioned direct approach. It is also often used to calibrate the results from pressure integration method for buildings with complex geometric shapes.

The performance of the closed-form formulations as compared to the numerical integrations of the response spectra for the response analysis is also examined. The error introduced by the closed-form formulations is less than 5%. As the wind load spectra determined from the time history data have certain variations, it is suggested to use the averaged spectrum over the half-power width around the modal frequency, i.e., twice of the damping ratio in terms of ratio of frequency to the modal frequency, to represent the spectrum at the modal frequency when using the closed-form formulations.

It is noted that the building top center accelerations in alongwind and acrosswind directions are almost uncorrelated. It can be readily explained from the closed-form formulation for the correlation coefficient of modal responses, Eqs. (12)-(15). The almost zero correlation is attributed to the uncorrelated alongwind and acrosswind loads. Without consideration of the correlation/coherence of the generalized forces, the modal correlation coefficient will not be correctly determined. It is different from the conventional uni-component earthquake excitations.

7. Influence of mode shape corrections on building responses: coupled case

The same tall building with an eccentricity of rigidity, i.e., the center of the rigidity at i th floor is located at $(e_{ixr}, e_{iyr}) = (-0.125B, -0.125B)$ is also considered. The centers of rigidity at different floors are on a single vertical line. As a result of eccentricity, the building exhibits 3D coupled mode shapes, particularly, strong coupled motion in two translational directions is observed. The modal shapes in term of the motions at the building top center $(x, y, 0.5B\theta)$ are $(-0.6550, 0.6550, 0.4612)$, $(0.7071, 0.7071, 0)$, and $(0.2663, -0.2663, 1.1346)$, respectively. The variation of the mode shapes over the building height follows a power law with an exponent of 1.25. The first and second fundamental modes are, respectively, dominated by the out-of-phase and in-phase coupled translational motions, indicating that the building approximately vibrates in the orthogonal diagonal directions of the building plan. The first mode is also coupled with in-plane torsional motion. The third mode is dominated by the torsional motion with coupled out-of-phase translations. The modal frequencies are 0.2088, 0.2300 and 0.3305 Hz. The damping ratio for each mode is assumed to be 1%.

Table 3 Comparison of the building responses (Coupled building, RMS)

Component	Approach	$X(cm)$	$Y(cm)$	$0.5B\theta(cm)$	CM_x	CM_y	CM_θ	CF_x	CF_y
$U_H = 20\ m/s$									
Mean	MPS	2.991	-0.143	-0.633	0.583	0	0	0.841	0
	HFFB	2.927	-0.140	-0.621	0.570	0	0	0.823	0
	Direct	3.028	-0.146	-0.643	0.589	0	0	0.851	0
B	MPS	0.553	0.764	0.197	0.108	0.153	0.027	0.156	0.221
	HFFB	0.563	0.782	0.194	0.110	0.157	0.031	0.159	0.227
	Direct	0.570	0.786	0.213	0.111	0.159	0.037	0.161	0.230
R	MPS	0.529	0.576	0.357	0.097	0.107	0.043	0.140	0.154
	HFFB	0.486	0.493	0.317	0.090	0.091	0.038	0.129	0.131
Total	MPS	0.765	0.957	0.407	0.145	0.186	0.051	0.210	0.269
	HFFB	0.744	0.924	0.372	0.142	0.182	0.049	0.205	0.263
$U_H = 40\ m/s$									
R	MPS	5.213	5.617	3.237	0.239	0.259	0.084	0.345	0.375
	HFFB	5.061	5.180	3.110	0.232	0.238	0.081	0.336	0.344
Total	MPS	5.663	6.395	3.331	0.262	0.301	0.088	0.379	0.435
	HFFB	5.539	6.050	3.205	0.257	0.285	0.087	0.371	0.412

Tables 3 and 4 summarize the response predicted by the MPS and HFFB approaches. It is noted that due to the coupling of the translation and torsion, the uncertainty introduced by the mode shape correlation for torsion is reduced. For instance, the error in the estimated building top torsional acceleration reduced to 10% from 22% in the uncoupled case at 20 m/s. The underestimations of alongwind acceleration and resultant acceleration at the corner A are reduced from 15% to 8%, and 13% to 8%, respectively.

In both uncoupled and coupled building cases, the contributions of the torsional acceleration to the acceleration at the building corner are two folds. It changes not only the magnitudes but also the correlation coefficient of the two translational acceleration components, thus the resultant acceleration.

Table 4 Comparison of the building accelerations (Uncoupled building, RMS, milli-g)

Approach	$(x, y) = (0, 0)$				$(x, y) = (0.5B, 0.5B)$				$0.5Ba_\theta$
	a_x	a_y	r_{xy}	$\sqrt{a_x^2 + a_y^2}$	a_x	a_y	r_{xy}	$\sqrt{a_x^2 + a_y^2}$	
$U_H = 20 \text{ m/s}$									
MPS	0.995	0.991	-0.23	1.124	1.538	1.529	-0.68	1.988	0.946
HFFB	0.928	0.942	-0.17	1.058	1.418	1.434	-0.64	1.826	0.738
$U_H = 40 \text{ m/s}$									
MPS	9.873	10.053	-0.16	11.272	14.715	14.947	-0.62	18.878	7.259
HFFB	9.633	9.866	-0.14	11.031	14.278	14.550	-0.61	18.291	7.003

8. Comparison of base moment/torque spectrum

In light of the significance of aerodynamic loads in the estimation of building responses, the reliability of aerodynamic base moment/torque spectra derived from the HFFB is important. There have been a number of studies concerning comparison of HFFB data. For example, the reliability of the measured spectra within the NatHaz Aerodynamic Load Database (NALD) (Zhou *et al.* 2003, Kwon *et al.* 2008) has been established through verifications against data sets from other wind tunnel experiments (Kareem 1989). The acrosswind spectra have been compared to a model derived from earlier measurements by Kareem (1988). Results in the torsional direction were also compared to those derived from pneumatic averaging, to overcome the uniform mode shape assumption inherent to the HFFB-derived torsional loads (Kareem 1990). Zhou *et al.* (2003) compared the NALD acrosswind loads with the empirical expression suggested by the Architectural Institute of Japan (AIJ 1996, Tamura *et al.* 1996). More recently, Kwon *et al.* (2008) compared the NALD data with empirical expressions of the acrosswind PSD (power spectral density) given in AIJ (1996, 2004) and Gu and Quan (2004).

In particular, it is worth noting that Lin *et al.* (2005) have provided an in-depth comparison of the NALD to their HFFB and SPM (synchronous pressure measurement) data sets. They noted that NALD's data was in close agreement with their studies with the exception of a few cases. They wrote, "With the linear mode shape assumption ... integrated simultaneous point pressures and HFFB agree for base force and moment spectra. NALD effectively provides the base moment spectra for preliminary design and can be expanded on the Internet by the data set here and by the other experimental results in the future." (Lin *et al.* 2005).

In this section, a summary of the expanded comparison of the base moment/torque spectra of

selected major studies in the alongwind, acrosswind and torsional spectra is presented, which is by no means exhaustive or meant to serve as a systematic comparison of HFFB data from different laboratories, codes and standards. Most wind tunnel studies have mainly focused on the acrosswind response due to generally its significance in most wind-sensitive buildings, therefore, information on the alongwind and torsional spectra is rather limited. Also, it is difficult to compare spectra among various studies due to different test conditions such as side ratio (D/B), aspect ratio ($AR=H/\sqrt{BD}$), boundary conditions (α), turbulence intensity, etc.

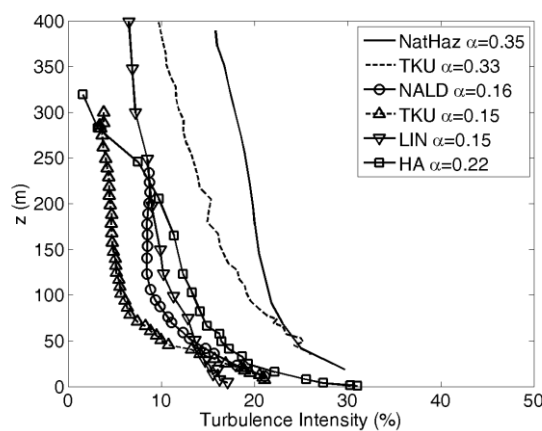


Fig. 5 Turbulence intensity profiles

Table 5 Experimental data used for comparison

NALD		Tamkang data ^[1]		Lin's data ^[2]		Ha's data ^[3]	
D/B	D/B	H/\sqrt{BD}	D/B	H/\sqrt{BD}	D/B	H/\sqrt{BD}	
0.33	–	–	0.34	4.00 (4.62)	0.33	6.00 (5.77)	
0.50	–	–	0.50	4.00 (3.77)	0.50	6.00 (5.66)	
0.67	–	–	0.63	4.00 (4.08)	0.67	6.00 (4.90)	
1.00	1.00	4.00, 5.00, 6.00 (6.00)	1.00	4.00, 5.00 (4.00, 5.00)	1.00	6.00 (6.00)	
1.50	1.50	7.00 (4.90)	1.59	4.00 (4.08)	1.50	6.00 (4.90)	
2.00	2.00	7.00 (5.66)	2.00	4.00 (3.77)	2.00	6.00 (5.66)	
3.00	3.00	7.00 (6.93)	2.98	4.00 (4.62)	3.00	6.00 (6.93)	

^[1] : Alongwind and acrosswind responses under two boundary conditions ($\alpha = 0.15, 0.33$)

^[2] : Alongwind, acrosswind and torsional responses under boundary condition ($\alpha = 0.15$)

^[3] : Acrosswind response under boundary condition ($\alpha = 0.22$)

Note: The values in the parentheses indicate corresponding NALD aspect ratios to be compared

In view of the preceding limitations, the following set of experimental data involving rectangular cross-sections was utilized; a) NALD (Zhou *et al.* 2003, Kwon *et al.* 2008): alongwind, acrosswind and torsional spectra based on HFFB in two boundary layers with $\alpha=0.16$ and 0.35 , similar to exposure C and A in ASCE 7-98/7-05); b) Tamkang data (Cheng and Wang 2004): alongwind and acrosswind spectral data using HFFB in two boundary conditions ($\alpha = 0.15$ and 0.33); c) Lin's data (Lin *et al.* 2005): SPM for alongwind, acrosswind and torsional spectra in $\alpha = 0.15$ (Note that they performed both HFFB and SPM in the case of $D/B = 1.0$); d) Ha's data (Ha *et al.* 2004): HFFB for $\alpha = 0.22$ (close to exposure B in ASCE 7-98/05) and $H/\sqrt{BD} = 6$. Turbulence intensity profiles of data sets are compared in Fig. 5 and clearly, there are some variations among these data sets. Table 5 summarizes features of the experimental data sets such as side ratio, aspect ratio and boundary conditions. It is noteworthy that these data sets have slight differences in side and aspect ratios and inflow boundary layer conditions such as the mean wind (α) and turbulence intensity profiles, which would lead to some discrepancies in the spectral comparison. The comparison of spectra is detailed in the following section.

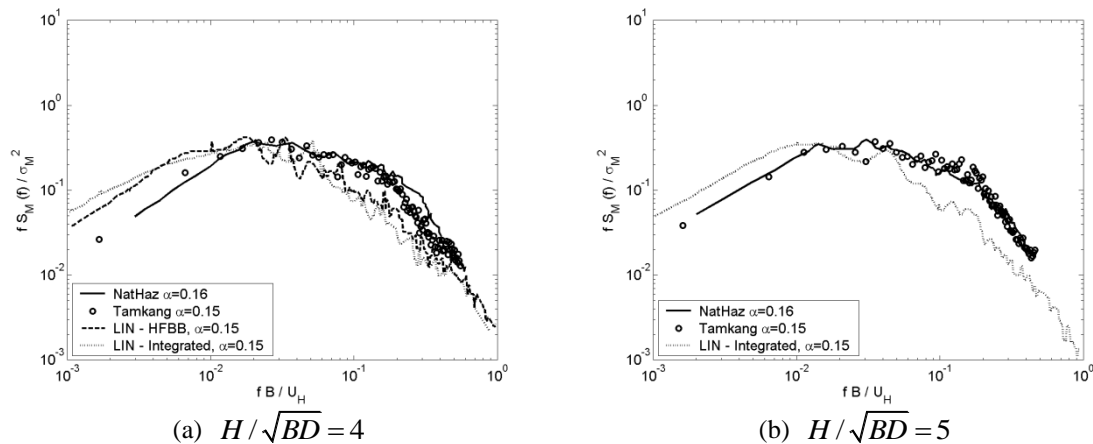


Fig. 6 Alongwind spectra in NALD, Tamkang and Lin's data ($D/B = 1.0$)

9. Acrosswind spectra

Overall, the acrosswind spectra in NALD, Tamkang and Lin's data show good agreement with one another as shown in Figs. 9 and 10. In addition, Ha's data is also compared to NALD and Tamkang data for $D/B = 1.5, 2.0$ and 3.0 (Fig. 11), even though inflow boundary layer in Ha's data set is a slightly different. Overall, Ha's data show trends similar to NALD under exposure A and Tamkang data shows some large peaks that may be attributed to difference in the aspect ratio of Tamkang data. A notable difference in Tamkang data for $D/B = 3.0$ in exposure C (Fig. 11(c)) exists. It may be due to the sensitivity of the flow around the cross-section as the side ratio is close to the 2.8 (e.g., Okajima 1982), which not only departs from the side ratio of $D/B = 3.0$ in this study but is also in the neighborhood of a critical value noted in Okajima (1982).

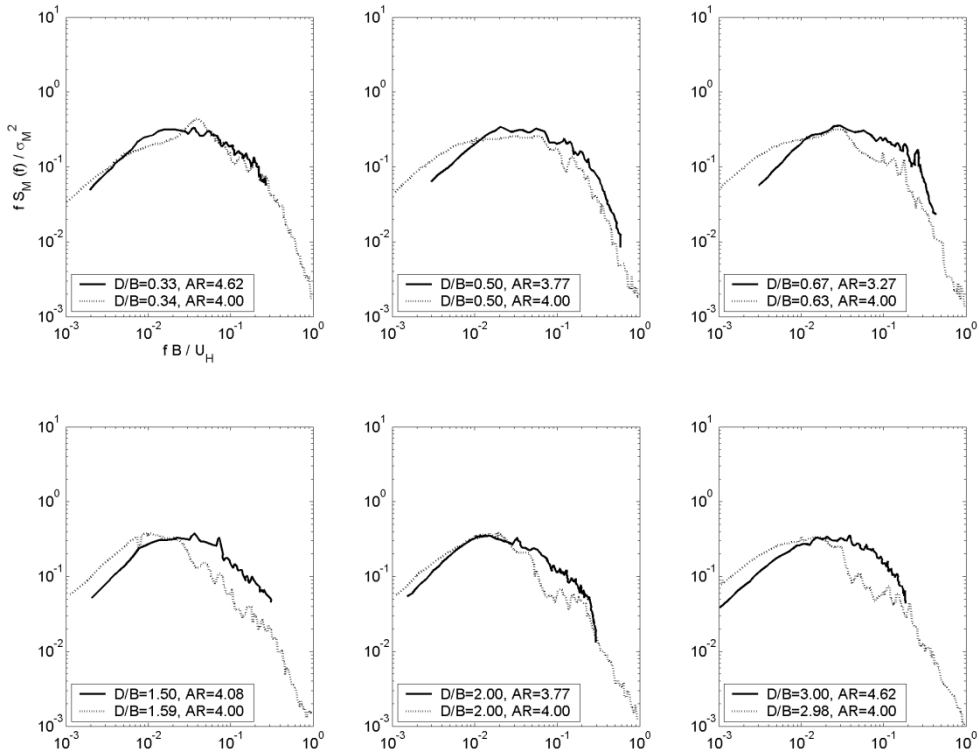


Fig. 7 Alongwind spectra in NALD (solid line) and Lin's data (dotted line) for various side ratios

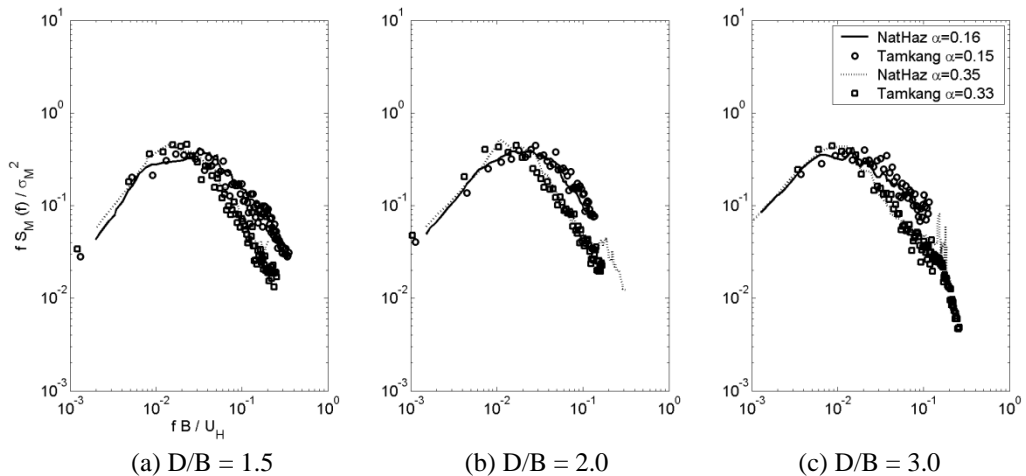


Fig. 8 Alongwind spectra in NALD and Tamkang data for two boundary conditions and various side ratios

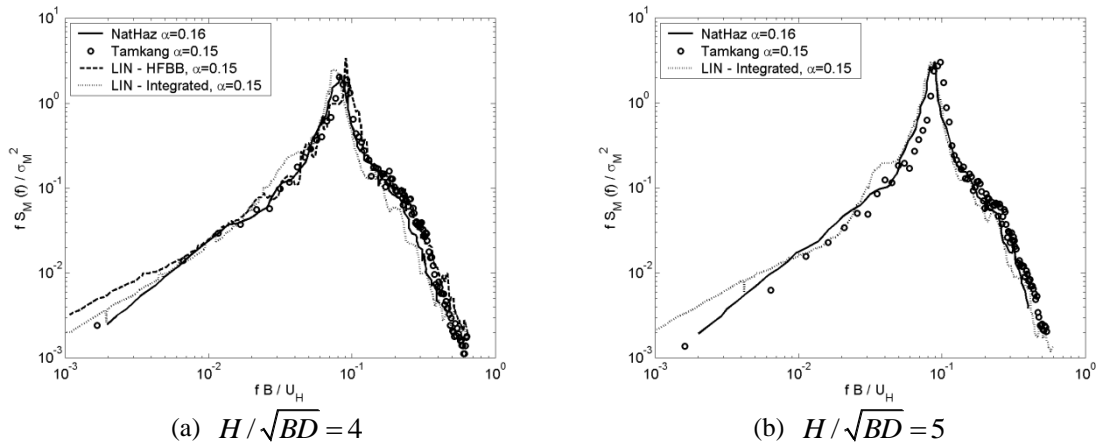


Fig. 9 Acrosswind spectra in NALD, Tamkang and Lin's data ($D/B = 1.0$)

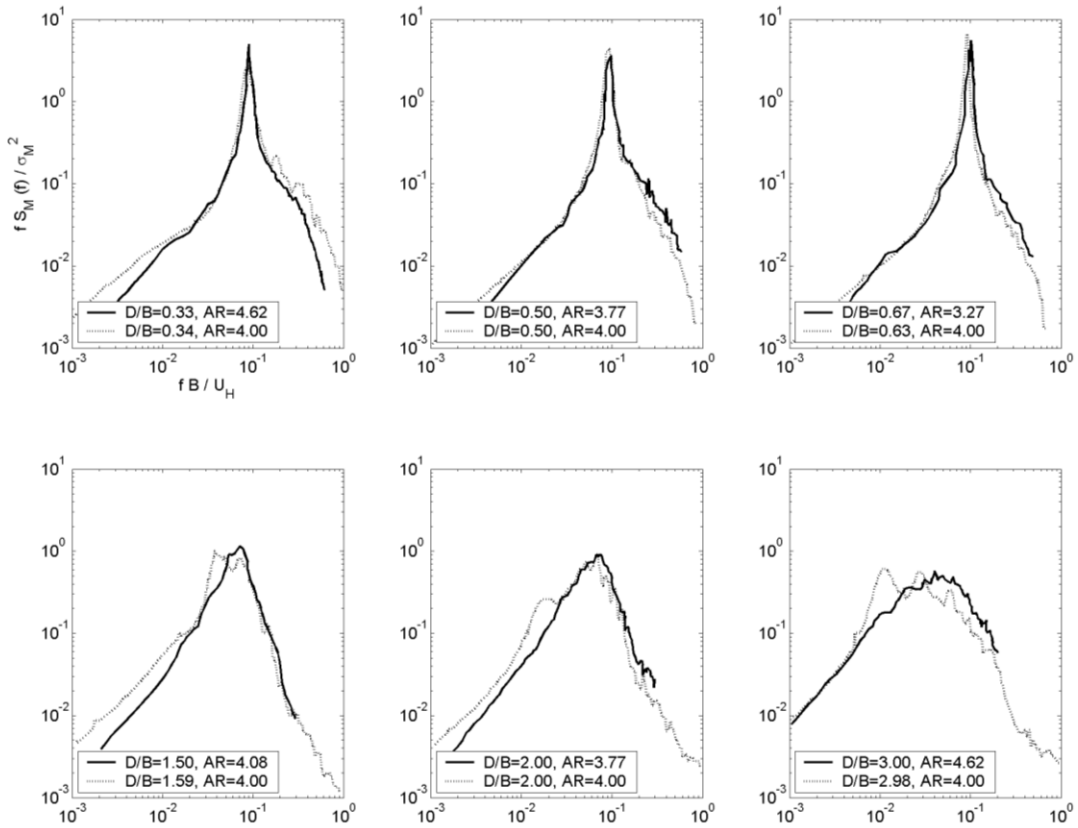


Fig. 10 Acrosswind spectra in NALD (solid line) and Lin's data (dotted line) for various side ratios

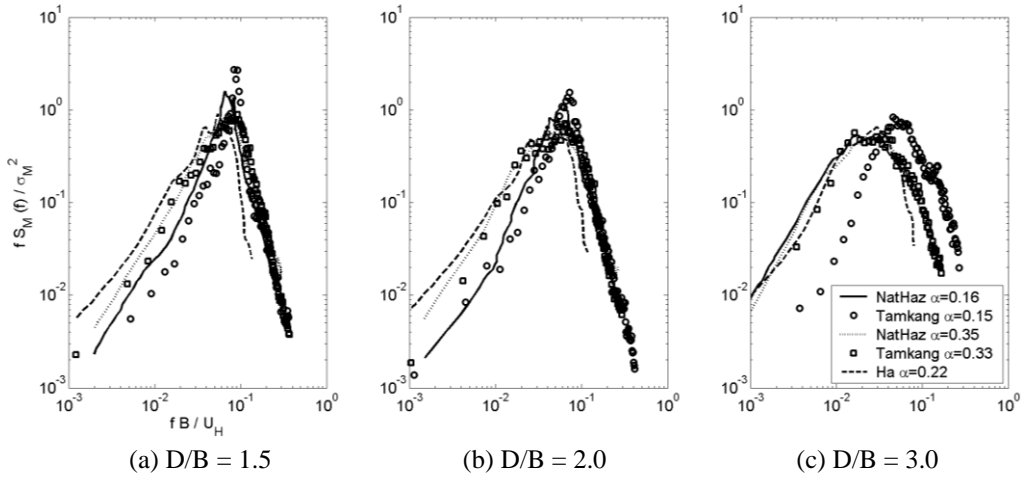


Fig. 11 Acrosswind spectra in NALD, Tamkang and Ha's data for various side ratios

Fig. 12 shows additional comparison of the acrosswind spectra in NALD and Ha's data for various side ratios ranging between 0.33 and 1.00. As observed in Fig. 11, most of Ha's data tends to show good agreement with NALD in exposure A despite slightly different aspect ratios (Table 5) and other test conditions not being exactly the same.

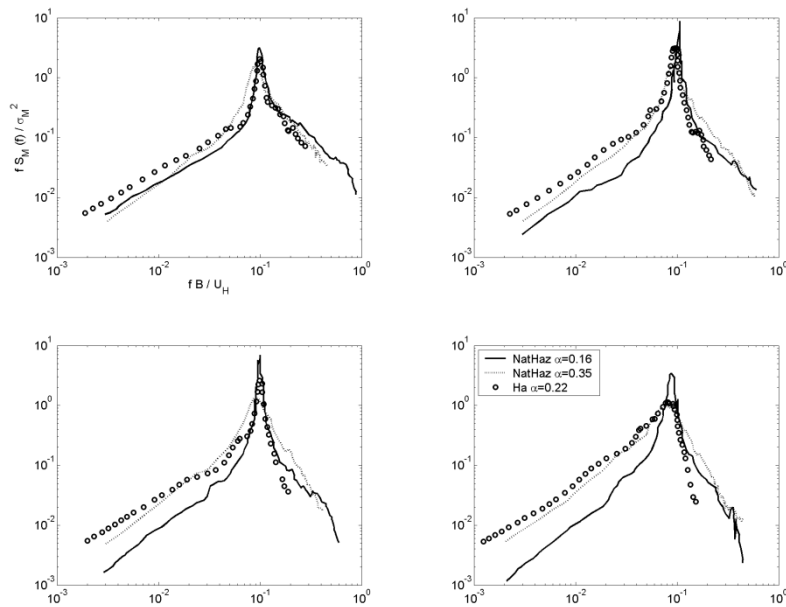


Fig. 12 Acrosswind spectra in NALD and Ha's data for various side ratios

The NALD crosswind spectra were also compared to the available empirical expressions. Fig. 13 shows NALD crosswind spectra and the empirical expressions in AIJ (1996, 2004) and Gu and Quan (2004) for $D/B = 1.0$ in both exposure A and C. It is noted that AIJ expressions are mainly functions of the side ratio (D/B) not reflecting inflow boundary layer condition and the building height explicitly, while Gu and Quan (2004) do represent those features. Regardless, NALD shows relatively good agreements with both empirical expressions even though discrepancies appear in the low-frequency range. These trends are also observed for $D/B = 2.0$ and $AR=3.75$ and 4.73 (Figs. 14(a) and 14(b)).

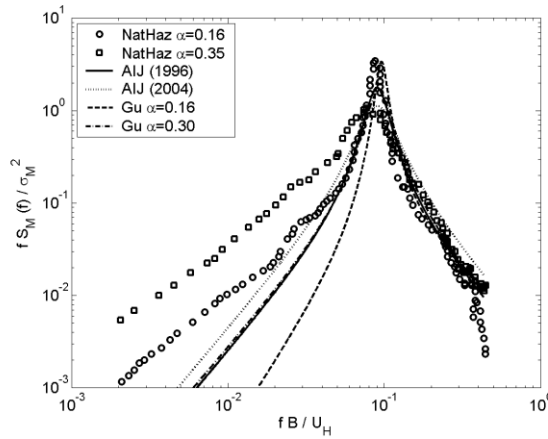
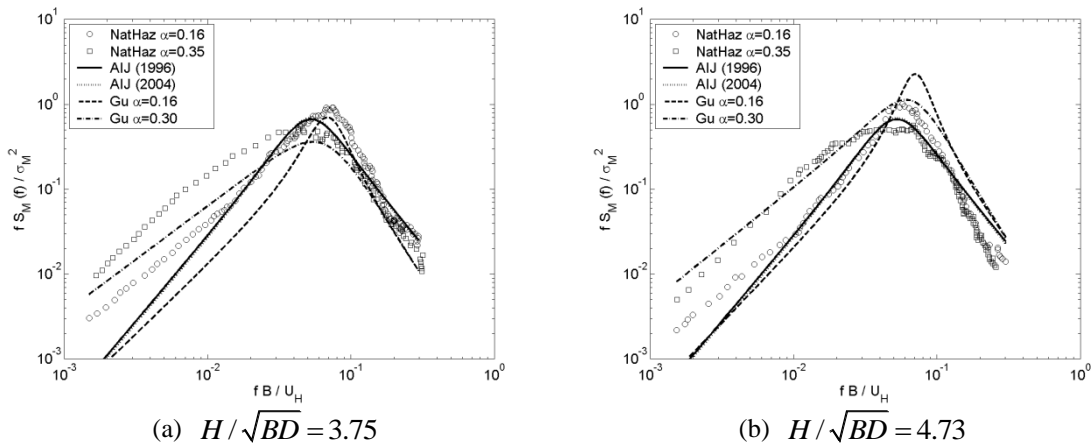


Fig. 13 NALD crosswind spectra with empirical expressions ($D/B = 1.0$)



(a) $H/\sqrt{BD} = 3.75$

(b) $H/\sqrt{BD} = 4.73$

Fig. 14 NALD crosswind spectra with empirical expressions ($D/B = 2.0$)

10. Torsional spectra

Due to a lack of torsional base moment spectra reported in the literatures, especially for different side ratios, a comparison of the experimental data is done only with NALD and Lin's data. Similar to the result for the along-wind direction for a square model ($D/B = 1.0$) (Fig. 6), the HFFB results show relatively lower values than those obtained from SPM at the peaks (Fig. 15), whereas the general trend has relatively good agreement (Fig. 16).

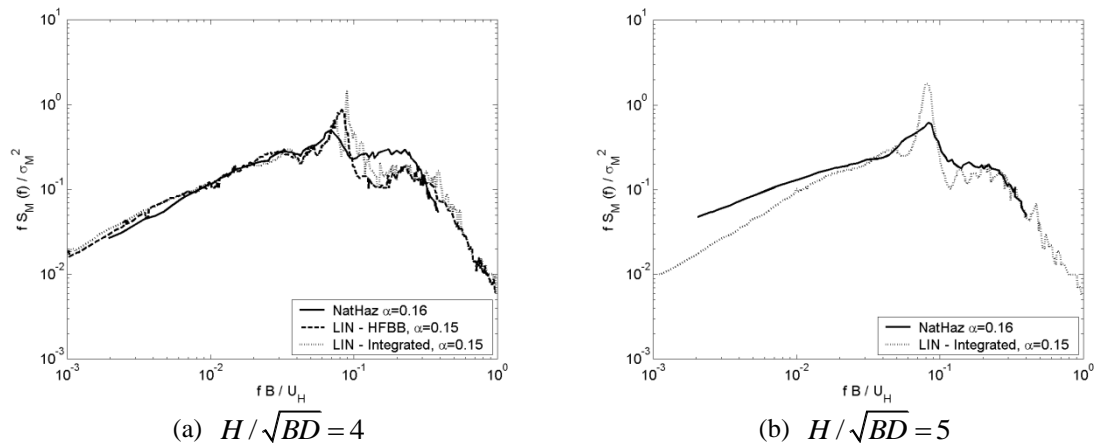


Fig. 15 Torsional spectra in NALD and Lin's data ($D/B = 1.0$)

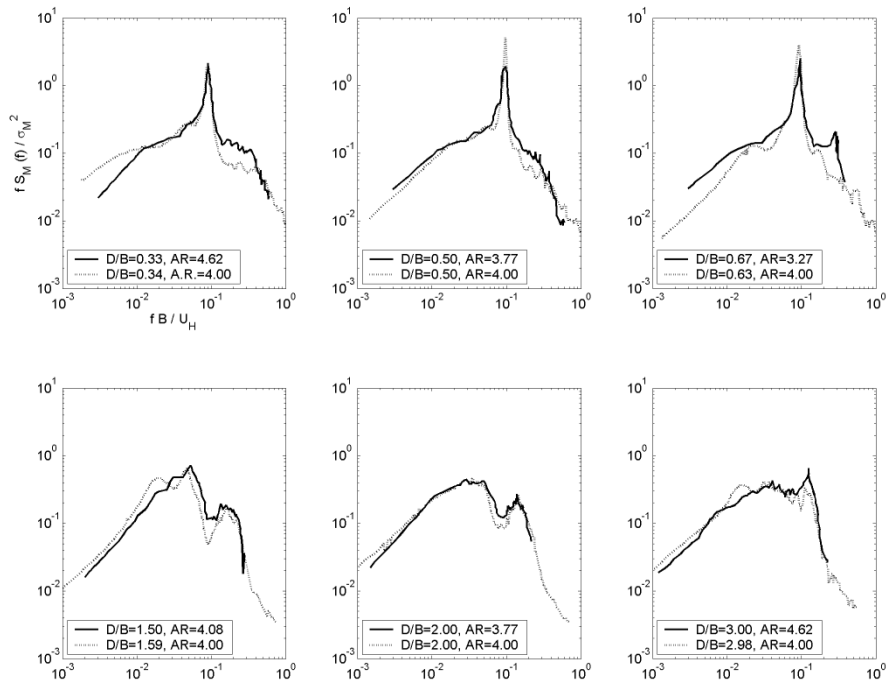


Fig. 16 Torsional spectra in NALD (solid line) and Lin's data (dotted line) for various side ratios

The NALD torsional spectra are also compared to the available empirical expression in AIJ (AIJ 2004) for six side ratios: 0.5, 0.67, 1.0, 1.5, 2.0 and 3.0 (Fig.17); Similar to the acrosswind case, the AIJ torsional expression does not reflect the flow conditions and building height but relies mainly on the side ratio (D/B). Note that the x -axis values in AIJ's torsional spectrum is defined in terms of $f/\sqrt{BD}/U_H$, which is converted to fB/U_H to match NALD. Due to this conversion, the expression is mostly shown in the high frequency ranges (Fig.17). Although some discrepancies are observed, the general trend of the overall NALD torsional spectra shows relatively good agreement with AIJ.

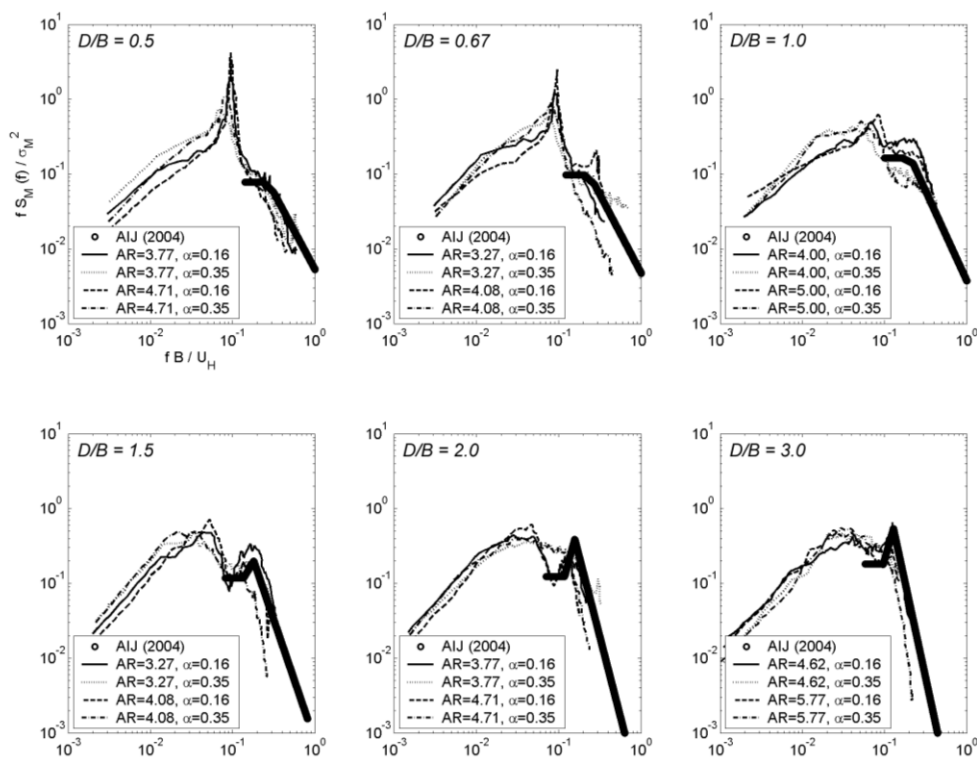


Fig. 17 NALD torsional spectra with AIJ empirical expression (AIJ 2004) for side ratios of 0.5, 0.67, 1.0, 1.5, 2.0 and 3.0

11. E-design/analysis based on HFFB data

Most codes and standards traditionally have relied on reductive formats and simplifications, which often lead to tables and plots to describe wind loads on structures. The level of accuracy inherent in codification information in this format and the uncertainty associated with interpolation or extrapolation of information may compromise the overall accuracy in code-specified load effects. This has led to database-enabled design procedures, which offer convenient meshing with existing analysis software. Primarily, such databases rely on wind tunnel derived data, which may be couched in analysis portals to provide desired load effects. Recent developments in

Internet/information technology (IT) offer attractive solutions to these challenges, allowing efficient means to collect, store, analyze, manage, and even share large data sets with the worldwide community (Kijewski *et al.* 2003, Kwon *et al.* 2005, Fritz and Simiu 2005).

The NatHaz Aerodynamic Loads Database (NALD) (<http://aerodata.ce.nd.edu>), first established in the fall of 2000 and recently re-designed, is an example of web-based database-enabled design using wind tunnel test data for the determination of alongwind, acrosswind and torsional response (Zhou *et al.* 2003, Kwon *et al.* 2008). This site has served as an important first step in establishing an on-line experimental database for use in the preliminary design of high-rise buildings which is being extensively consulted by a number of firms (e.g., McNamara 2005) and individual researches (e.g., Chan and Chui 2006).

The NALD has utilized a combination of web-based programming tools and popular engineering software based on information/Internet technologies, e.g., Apache web servers, JAVA/JavaScript, Hypertext Preprocessors (PHP), Structured Query Language databases (MySQL) and MATLAB. It offers more attractive and user-friendly features to allow not only the retrieval of power spectral values at specific reduced frequencies, but also the on-line determination of resulting base moments and equivalent static wind loads (ESWL) for survivability and accelerations for serviceability (habitability) considerations. Thus in NALD, a dual purpose design aid is introduced: a database-driven web archive of HFFB data and a stand-alone analysis engine that can be used independently or in tandem for estimating ESWL and building dynamic response. The NALD portal has been introduced in the commentary of ASCE 7-05 (C6.5.8) to provide guidance for accessing dynamic wind induced loads on a suite of generic isolated buildings.

The user-friendly interface (Fig.18) allows the selection of a desired test case in only one step with additional options for specifying the input power spectral density (PSD) expressed by reduced frequency and non-dimensional base moment/torque spectrum. At present, three user options are available for prescribing a PSD for the analysis: PSD data from the NALD (default option), a user-specified PSD (curve-fitted or analytical expression) or user-supplied PSD data (X, Y data pairs). After selecting these basic inputs, the module requests additional inputs for the full-scale system, including cross-sectional dimensions, height, exposure category, and fundamental dynamic characteristics. Either Metric (SI) or English units may be specified for the structural inputs and calculated outputs; note that an on-line unit conversion module is also provided for users' convenience in unit inputs.

In terms of MATLAB as the computational tool for the background design/analysis, the following quantities are then displayed on the result interface: non-dimensional spectral base moment/torque, wind speeds for both survivability (50-year mean recurrence interval) and serviceability (10-year mean recurrence interval) in the exposure of interest, RMS base moment coefficient, non-dimensional moment coefficient, base moment and the maximum alongwind and acrosswind displacements for survivability design, 10-year RMS and peak alongwind and acrosswind accelerations, corresponding lateral accelerations induced by torsion, and total lateral accelerations at the corner. All displacements and accelerations are calculated at the roof level. All these quantities, i.e., base bending moments, displacements and accelerations, are displayed for each of the three response components (Fig. 19). Finally, a plot of the mean, background and resonant components of the ESWL on the building are displayed for the end-user, as shown in Fig. 20. As such, the NALD can be also used to express wind loads, i.e., the ESWL in three directions in terms of 3-D gust loading factors (GLF), akin to the along wind GLF (Kareem and Zhou 2003, Tamura *et al.* 2005).

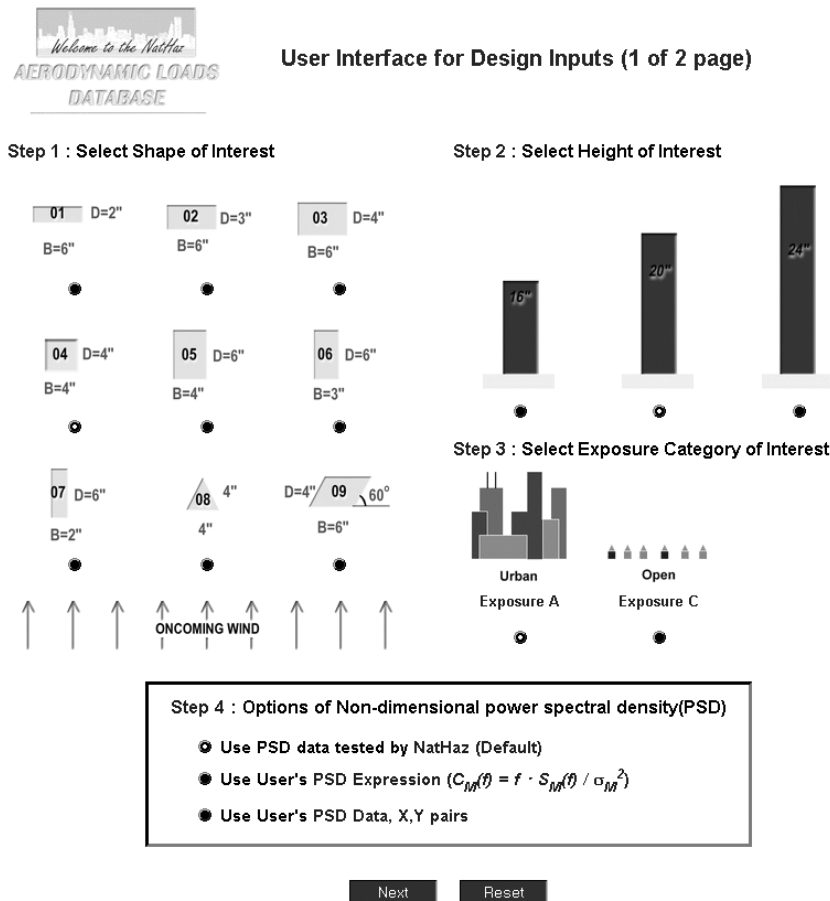


Fig. 18 NALD data selection menu for on-line analysis, including PSD option

It should again be emphasized that one unique feature provided by this on-line analysis module is the user's options for providing the non-dimensional PSD. Depending on the selected PSD option specified in Fig. 18, additional inputs will be requested following the prompt for structural inputs with the supplemental interface such as user-supplied PSD expressions and user-supplied PSD data sets of X (reduced frequency) and Y (non-dimensional base moment PSD) pairs. More details and screenshots of the web interface can be found in Kwon *et al.* (2008). Since this on-line analysis module mainly utilizes MATLAB, the aforementioned inputs should be MATLAB compatible. The "Info link" displayed in the top line provides the user with simple guidelines to minimize unexpected input errors. The on-line analysis module also includes a simple error-detection scheme with pop-up error messages, which alert users if input values are beyond the NALD's range of applicability. The provision for PSD options extends the utility of NALD by offering an on-line dynamic analysis framework that can be utilized for estimating dynamic load effects on high-rise buildings with alternative input options, e.g., an independent wind tunnel study or empirical expression from any wind load standard. This versatility provides users with a robust stand-alone, on-line analysis engine that offers the flexibility option of utilizing user-supplied

custom spectral description or wind tunnel test (HFFB) results to provide final design estimates of wind load effects on buildings and permit comparative studies of predictions from various sources.

■ **Survivability Design (50-year wind) : Base moments**

	Base Moment (10^6 kN-m)			
	\bar{M}	\hat{M}_B	\hat{M}_R	\hat{M}
Alongwind	1.2828	0.9734	1.4828	3.0566
Acrosswind	-	1.1899	3.6403	3.8298
Torsional	-	0.0784	0.1386	0.1592

■ **Survivability Design (50-year wind) : Maximum Displacements**

	Maximum Displacements at roof
Alongwind	0.363 m
Acrosswind	0.455 m

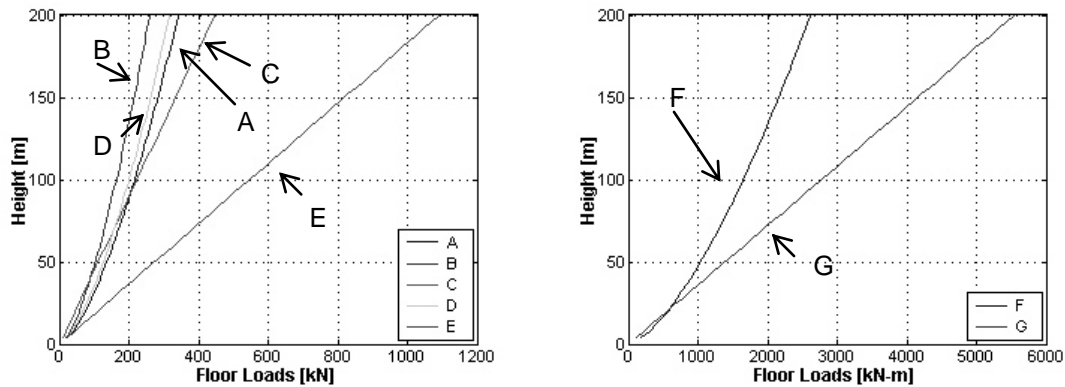
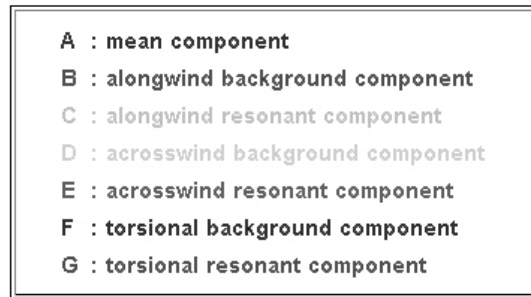
■ **Serviceability Design (10-year wind) : Peak and RMS Accelerations**

	Peak Accelerations at roof	
Alongwind	14.19 milli-g	
Acrosswind	23.50 milli-g	
Lateral Accelerations at Corner Induced by Torsion	0.00476 rad/s ²	Alongwind component : 9.70 milli-g
		Acrosswind component : 9.70 milli-g
Total Lateral Accelerations at Corner	Alongwind component : 17.19 milli-g Acrosswind component : 25.43 milli-g	

	RMS Accelerations at roof	
Alongwind	3.75 milli-g	
Acrosswind	6.21 milli-g	
Lateral Accelerations at Corner Induced by Torsion	0.00121 rad/s ²	Alongwind component : 2.47 milli-g
		Acrosswind component : 2.47 milli-g
Total Lateral Accelerations at Corner	Alongwind component : 4.49 milli-g Acrosswind component : 6.68 milli-g	

Fig. 19 Display of on-the-fly calculated survivability and serviceability values

■ Wind Force Components(mean, background and resonant components)



■ Download data file including all wind force components : w_force_all_ml00001.dat
(Column 1 : heights [m], Column 2 to 8 : wind force component A to G [kN, kN-m])

Fig. 20 Display of on-the-fly calculated wind force components

12. Conclusions

A general analysis framework for buildings with 3D coupled mode shapes with HFFB technique was addressed. A total of nine mode shape corrections were needed for quantifying the generalized forces from the HFFB measurements. These empirical corrections can be estimated using the same formulations for buildings with uncoupled mode shapes. The accuracy of the mode shape corrections used in practice was examined using the scanning of pressures on a square tall building. The results showed that the correlations for the translational loads were very accurate. It was due, in part, to the similarity of the linear influence function of the base bending moment to the translational mode shape. On the other hand, as the uniform influence function of the base

torque departs considerably from the mode shape shape in torsion, the mode shape correlation for torsional load remains a challenge with a larger uncertainty. This uncertainty is similar to the estimation of the translational load from the measurement of base shear force rather than the bending moment.

The influence of the uncertainty in mode shape corrections to different building responses were examined for both uncoupled and coupled cases. The uncertainty in the torsional load can noticeably affect the building top acceleration at corners. The torsional acceleration contributes not only the magnitudes but also the correlation of the translational accelerations thus the magnitude of the resultant acceleration. As compared to the uncoupled case, the influence of the uncertainty in mode shape corrections on coupled building response was reduced. Such an influence depends on the wind load characteristics and building dynamics.

An alternative approach was introduced for estimating the mean and background response components from the HFFB measurements without mode shape corrections. The effectiveness of this approach was demonstrated for both uncoupled and coupled buildings. It should be noted that, due to limited loading information with the HFFB technique, the mean and background response components have to be estimated using the modal analysis involving the three fundamental modes. As compared to the resonant component, the predicted mean and background components are less accurate as they are generally more sensitive to the higher mode contributions. The base shear and base torque are more influenced by the higher mode contributions as compared to the building top displacement, acceleration and base bending moment. The sensitivity of the building response to the higher modes depend on the influence function of the response.

A comparison of the base moment/torque spectra in the alongwind, acrosswind and torsional directions utilizing the HFFB reported in selected major studies was presented. It was by no means exhaustive or meant to serve as a systematic comparison of HFFB data from different laboratories, codes and standards but offered a representative glimpse of the variations among these measurements. Overall, relatively good agreements, despite different test conditions, were observed. Following the comparison, the e-technology aspect of NatHaz Aerodynamic Loads Database (NALD) (<http://aerodata.ce.nd.edu>) was highlighted, which facilitates the use of HFFB data for preliminary design stages of tall buildings subjected to wind loads. This unique e-version of the database enabled design feature is particularly useful for those who may not be very familiar with the details of the dynamic analysis procedure, but are employed in the response estimation of wind-sensitive structures. In addition, the robust framework presented here is conveniently amenable to immediate expansion.

Acknowledgments

The first author is grateful for the financial support in part by National Science Foundation (Grant No. CMS 08-24748). The second and third authors wish to acknowledge Drs. Chii-Ming Cheng and Jenmu Wang, Tamkang University, Taiwan for their contributions. The second and third authors are also grateful for the financial support in part by the National Science Foundation (Grant No. CMMI 03-24331, CMMI 06-01143 and CBET 07-42191) and the Global Center Of Excellence (GCOE) at Tokyo Polytechnic University, Tokyo funded by MEXT.

References

- Architectural Institute of Japan (AIJ) (1996, 2004), *Recommendations for loads on buildings*, Architectural Institute of Japan.
- American Society of Civil Engineers (ASCE) (1998), *Minimum design loads for buildings and other structures*, ASCE 7-98, ASCE, Reston, VA.
- American Society of Civil Engineers (ASCE) (2005), *Minimum design loads for buildings and other structures*, ASCE 7-05, ASCE, Reston, VA.
- Boggs, D.W. and Peterka, J.A. (1989), "Aerodynamic model tests of tall buildings", *J. Eng. Mech. - ASCE*, **115**(3), 618-635.
- Chan, C.M. and Chiu, J.K.L. (2006), "Wind-induced response and serviceability design optimization of tall steel buildings", *Eng. Struct.*, **28**(4), 503-513.
- Chen, X., and Huang, G. (2009), "Evaluation of peak resultant response for wind-excited tall buildings." *Eng. Struct.*, **31**(4), 858-868.
- Chen, X. and Kareem, A. (2001), "Equivalent static wind loads for buffeting response of bridges", *J. Struct. Eng. - ASCE*, **127**(12), 1467-1475.
- Chen, X. and Kareem, A. (2004), "Equivalent static wind loads on tall buildings: new model", *J. Struct. Eng. - ASCE*, **130**(10), 1425-1435.
- Chen, X. and Kareem, A. (2005a), "Coupled dynamic analysis and equivalent static wind loads on buildings with three-dimensional modes", *J. Struct. Eng. - ASCE*, **131**(7), 1071-1082.
- Chen, X. and Kareem, A. (2005b), "Dynamic wind effects on buildings with 3D coupled modes: application of high frequency force balance measurements." *J. Eng. Mech. - ASCE*, **131**(11), 1115-1125.
- Cheng, C.M. and Wang, J. (2004), "Wind tunnel database for an intermediate wind resistance design of tall buildings", *Proceedings of the 1st International Symposium on Wind Effects on Buildings and Urban Environment*, Tokyo Polytechnic University, Tokyo, Japan.
- Davenport, A.G. (1967), "Gust loading factors." *J. Struct. Eng. - ASCE*, **93**, 11-34.
- Davenport, A.G. (1985), "The representation of the dynamic effects of turbulent wind by equivalent static wind loads", *Proceedings of the AISC/CISC Int. Symp. on Struct. Steel*, Chicago.
- Davenport, A.G. (1995), "How can we simplify and generalize wind loads?," *J. Wind Eng. Ind. Aerod.*, **54-55**, 657-669.
- Flay, R. G. J., Yip, D. Y. N., and Vickery, B. J. (1999), "Wind induced dynamic response of tall buildings with coupled 3D modes of vibration", *Proceedings of the 10th Int. Conf. on Wind Eng.*, Copenhagen, Denmark.
- Fritz, W.P. and Simiu E. (2005), "Probabilistic description of tall building response to wind: Database-assisted design, dynamics, and wind directionality effects", *Proceedings of the 9th International Conference on Structural Safety and Reliability*, Rome, Italy.
- Gu, M. and Quan, Y. (2004), "Across-wind loads of typical tall buildings", *J. Wind Eng. Ind. Aerod.*, **92**(13), 1147-1165.
- Ha, Y.C., Kim, D.W. and Kil, Y.S. (2004), "Characteristics of the across-wind fluctuating force and spectral density of rectangular high-rise buildings with various side ratios", *Proceedings of the CTBUH 2004*, CTBUH, Seoul, Korea.
- Holmes, J.D. (2002), "Effective static load distributions in wind engineering", *J. Wind Eng. Ind. Aerod.*, **90**, 91-109.
- Holmes, J.D., Rofail, A. and Aurelius, L. (2003), "High frequency base balance methodologies for tall buildings with torsional and coupled resonant modes", *Proceedings of the 11th Int. Conf. on Wind Eng.*, Lubbock, TX, Texas Tech University.
- Huang, G. and Chen, X. (2007), "Wind load effects and equivalent static wind loads of tall buildings based on synchronous pressure measurements", *Eng. Struct.*, **29**(10), 2641-2653.
- Irwin, P.A. and Xie, J. (1993), "Wind loading and serviceability of tall buildings in tropical cyclone regions", *Proceedings of the 3rd Asia-Pacific Symp. on Wind Eng.*, Hong Kong, University of Hong Kong.

- Islam, S., Ellingwood, B. and Corotis, R.B. (1992), "Wind-induced response of structurally asymmetric high-rise buildings", *J. Struct. Eng. - ASCE*, **118**(1), 207-222.
- Kareem, A. (1985), "Lateral-torsional motion of tall buildings to wind loads", *J. Struct. Eng. - ASCE*, **111**(11), 2479-2496.
- Kareem, A. (1988), "Measurements and analysis of pressure fluctuations on prismatic structures in turbulent boundary layer flows", *J. Wind Eng. Ind. Aerod.*, **137**, 229-235.
- Kareem, A. (1989), "Mapping and synthesis of random pressure fields", *J. Eng. Mech. - ASCE*, **115**(10), 2325-2332.
- Kareem, A. (1990), "Measurement of pressure and Force fields on building models in simulated atmospheric flows", *J. Wind Eng. Ind. Aerod.*, **36**(1), 589-599.
- Kareem, A. and Cermak, J.E. (1979), "Wind tunnel simulation of wind-structure interactions", *ISA T.*, **18**(4), 23-41.
- Kareem, A. and Zhou, Y. (2003), "Gust loading factors - past, present and future", *J. Wind Eng. Ind. Aerod.*, **91**(12-15), 1301-1328.
- Kijewski, T., Kwon, D. and Kareem, A. (2003), "E-Technologies for wind effects on structures", *Proceedings of the 11th Int. Conf. on Wind Eng.*, Wind Science and Engineering Research Center, Texas Tech University, Lubbock, TX.
- Kwon, D., Kijewski-Correa, T. and Kareem, A. (2005), "e-analysis/design of tall buildings subjected to wind loads", *Proceedings of the 10th Americas Conf. on Wind Eng.*, AAWE.
- Kwon, D., Kijewski-Correa, T. and Kareem, A. (2008), "e-analysis of high-rise buildings subjected to wind loads", *J. Struct. Eng. - ASCE*, **134**(7), 1139-1153.
- Lin, N., Letchford, C., Tamura, Y., Liang, B. and Nakamura, O. (2005), "Characteristics of wind forces acting on tall buildings", *J. Wind Eng. Ind. Aerod.*, **93**(3), 217-242.
- McNamara, R.J. (2005), *Some current trends in high rise structural design*, STRUCTURE magazine, September, 19-23.
- Okajima, A. (1982), "Strouhal numbers of rectangular cylinders", *J. Fluid Mech.*, **123**, 379-398.
- Reinhold, T.A. and Kareem, A. (1986), "Wind loads and building response predictions using force balance techniques", *Proceedings of the 3rd ASCE Eng. Mech. Conf. - Dynamics of Structures*, UCLA.
- Repetto, M.P. and Solari, G. (2004), "Equivalent static wind actions on vertical structures", *J. Wind Eng. Ind. Aerod.*, **92**(5), 335-357.
- Shimada, K., Tamura, Y., Fujii, K. and Wakahara, T. (1990), "Wind induced torsional motion of tall building", *Proceedings of the 11th National Symp. on Wind Eng.*, Tokyo, (In Japanese).
- Tamura, Y., Kareem, A., Solari, G., Kwok, K.C.S. and Holmes, J.D. (2005), "Aspects of the dynamic wind-induced response of structures and codification", *Wind Struct.*, **8**(4), 251-268.
- Tamura, Y., Kawai, H., Uematsu, Y., Marukawa, H., Fujii, K. and Taniike, Y. (1996), "Wind load and wind-induced response estimations in the Recommendations for Loads on Buildings, AIJ 1993", *Eng. Struct.*, **18**(6), 399-411.
- Tamura Y., Suganuma, S., Kikuchi, H. and Hibi, K. (1999), "Proper orthogonal decomposition of random wind pressure field", *J. Fluid Struct.*, **13**, 1069-1095.
- Tallin, A. and Ellingwood, B. (1985), "Wind induced lateral-torsional buildings", *J. Struct. Eng. - ASCE*, **111**(10), 2197-2213.
- Tschanz, T. and Davenport, A.G. (1983), "The base balance technique for the determination of dynamic wind loads", *J. Wind Eng. Ind. Aerod.*, **13**(1-3), 429-439.
- Vickery, B.J. and Basu, R.I. (1984), "The response of reinforced concrete chimneys to vortex shedding", *Eng. Struct.*, **6**, 324-333.
- Vickery, P.J., Steckley, A.C., Isyumov, N. and Vickery, B.J. (1985), "The effect of mode shape on the wind induced response of tall buildings", *Proceedings of the 5th U.S. National Conf. on Wind Eng.*, Texas Tech. University, Lubbock, TX.
- Xie, J. and Irwin, P.A. (1998), "Application of the force balance technique to a building complex", *J. Wind Eng. Ind. Aerod.*, **77-78**, 579-590.
- Xie, J., Kumar, S. and Gamble, S. (2003), "Wind loading study for tall buildings with similar dynamic

- properties in orthogonal directions”, *Proceedings of the 10th Int. Conf. on Wind Eng.*, Copenhagen, Denmark.
- Xu, Y.L. and Kwok, K.C.S. (1993), “Mode shape corrections for wind tunnel tests of tall buildings”, *Eng. Struct.*, **15**, 618-635.
- Yip, D.Y.N. and Flay, R.G.J. (1995), “A new force balance data analysis method for wind response predictions of tall buildings”, *J. Wind Eng. Ind. Aerod.*, **54-55**, 457-471.
- Zhou, Y. and Kareem, A. (2001), “Gust loading factor: new model”, *J. Struct. Eng. - ASCE*, **127**(2), 168-175.
- Zhou, Y. and Kareem, A. (2003), “Aeroelastic balance”, *J. Eng. Mech. - ASCE*, **129**(3), 283-292.
- Zhou, Y., Kareem, A. and Gu, M. (2002), “Mode shape corrections for wind load effects”, *J. Eng. Mech. - ASCE*, **128**(1), 15-23.
- Zhou, Y., Kijewski, T. and Kareem, A. (2002), “Along-wind load effects on tall buildings: comparative study of major international codes and standards”, *J. Struct. Eng. - ASCE*, **128**(6), 788-796.
- Zhou, Y., Kijewski, T. and Kareem, A. (2003). “Aerodynamic loads on tall buildings: Interactive database”, *J. Eng. Mech. - ASCE*, **129**(3), 394-404.